Continuous Casting Consortium
Report to POSCO

Modeling Steel Slab Heat Transfer During Scarfing Processing

Xiaoxu Zhou
Brian G. Thomas

July 30, 2010

Department of Mechanical Science and Engineering
University of Illinois at Urbana-Champaign

Section I. Abstract

The scarfing processing experiment was carried out for a steel slab moving at a constant speed with the scarfing torch fixed. The temperature histories inside the slab were recorded by two sets of thermocouples in different depths. A two-step computational model of heat transfer in scarfing processing has been developed in FLUENT. The model features in detail heat conduction from both the hot slag coating and the scarfing reaction to the steel slab surface, and it solves for steady state heat advection in the Step-1 model followed by the Step-2 model of transient heat transfer calculation. The combination of these two steps is able to give the complete prediction of a temperature history of 122.2 sec. The temperature predictions agree well with the experimental measurements. The high temperature region (1100 ^{o}C ~ 1500 ^{o}C) is found to be mainly located in a depth of 0.5 mm near the slab surface. The fraction of heat conducted from the hot slag coating into the slab is 5.4% while that from the scarfing reaction is 10.3%. The simulations clearly explain the measurements and suggest practical implications.

Section II. Background

Scarfing processing has been used widely to remove surface defects from steel and other semi-finished as-cast products for over 70 years. The first automated scarfing machine used in production was built and installed in 1935. Steel slabs produced from continuous casting often exhibit surface defects, including inclusions, pits and cracks, such as shown in Fig. 1. In order to obtain advanced high strength steels (AHSS) for automotive parts or other high-quality-products, these surface defects should be avoided during the casting process or removed during post-processing using the scarfing technique.

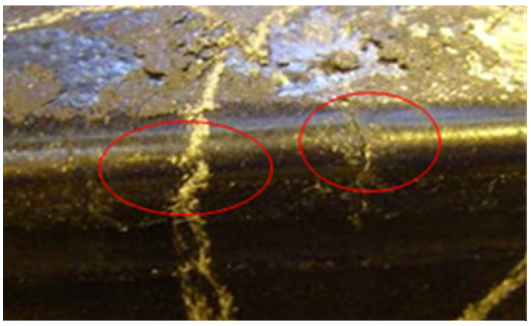

Fig. 1 Transverse Corner Cracks from Continuously Cast Steel Slab

As shown in Fig. 2, the gas fuel (such as propane C_3H_8) and oxygen leaving the torch combust into a high temperature flame, which heats the slab sufficiently to initiate the exothermic reaction of iron with available excess oxygen to form iron oxide (mainly $3Fe+2O_2=Fe_3O_4+972.4$ KJ/mol [Appendix A] for reactants and products at 1500 ^oC [1], calculated using Kirchhoff's law). During this scarfing reaction, part of the released heat increases the temperature and melts the iron oxide products (FeO, Fe_2O_3, Fe_3O_4) [2,3], part of the heat is transported away through radiation and advection with the combustion gas and the rest is conducted into the steel slab. Most of the iron oxides are swept away by the high-speed oxygen and combustion gases as soon as they form, but some of this material remains in liquid slag form which is blown across the surface of the steel slab as an intermittent coating layer. The hot liquid slag coating layer, shown in Fig. 2, conducts some heat into the steel slab and provides some preheat for the continuous scarfing reaction process.

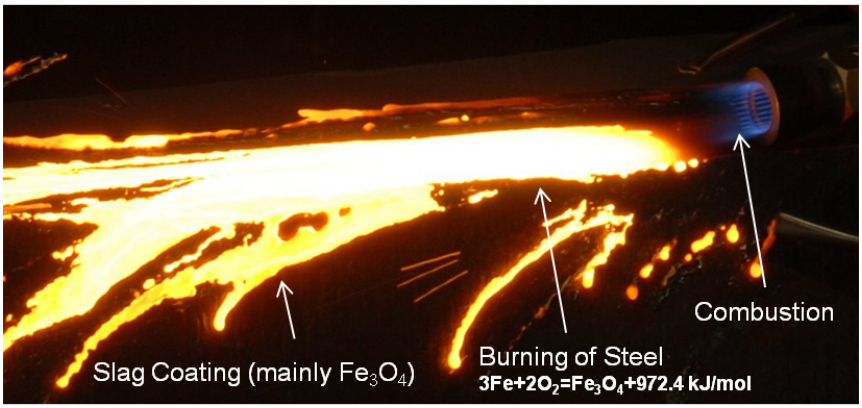

Fig. 2 Scaring Processing along the Steel Slab Corner

In scarfing to remove corner cracks, the torch moves forward along the slab, such as shown in Fig. 3. The new curved surface or "scarfing surface", or "final surface" created by the scarfing process shows that ~25mm depth of steel has been removed from the corner. The slag droplets that scatter and spread across both the top and side surfaces are also shown clearly in Fig. 3. Note that these slag layers become more intermittent with distance from the corner surface. The corner region is covered with a relatively continuous slag coating, while further regions experience some uncovered spots.

Fig. 3 Slag Coatings after the Scarfing Processing

Previous literature on scarfing processing mainly focuses on the design or optimization of the scarfing machines [4~10]. Very few papers are concerned with quantifying or modeling the fundamental phenomena which govern the process, including the complex inter-related gas flow, combustion, material removal, melting, and various heat transfer mechanisms during scarfing. In Rawson's technical report [11], an analytical solution of one-dimensional heat conduction into the steel slab was attempted for scarfing of a flat face. Showalter [12] summarized the basic fundamental concepts of scarfing including the heat transfer mechanisms, fluid dynamics and chemical reactions and proposed a simple analytical solution to calculate the scarfing depth by balancing heat between the flame, slag, oxidization, and sensible heat of the slab. No previous work has considered scarfing along an edge. Furthermore, no computational modeling of the scarfing processing has been performed, owing to the high difficulty and modeling complexity of the associated physical phenomena.

This report presents a fundamental three-dimensional computational heat-transfer model of the scarfing process and applies it to provide a detailed description of the heat transfer mechanisms. The model is calibrated to match experimental measurements of the controlled scarfing process at POSCO and the results are analyzed to quantify the partitioning of heat during the process.

Section III. Experiment

A controlled instrumented scarfing experiment was performed on a thick steel slab at Pohang Iron and Steel Company (POSCO) [13]. The slab dimensions, shown in Fig. 4, feature a total length of 1200 mm and a 250 x 250 mm cross section with the left bottom chopped off. The steel composition is listed in Table 1.

Elements	C	Al	Si	Cu	Mn	Nb	P	N	S
wt%	0.07516	0.03286	0.22320	0.02754	1.25600	0.02590	0.01520	0.00330	0.00202

Table 1 Steel Composition

Two sets of nine thermocouples (TCs) were installed respectively in two cross sections separated by 65 mm as indicated by the thick vertical lines in Fig. 4. Each set was oriented in a U-shape around the corner, anticipating the material removed by scarfing. TC set 1 (TC11-TC19) has an approximate depth of 5 mm from the slab surface after scarfing while the TC set 2 (TC21-TC29) has an approximate depth of 10 mm.

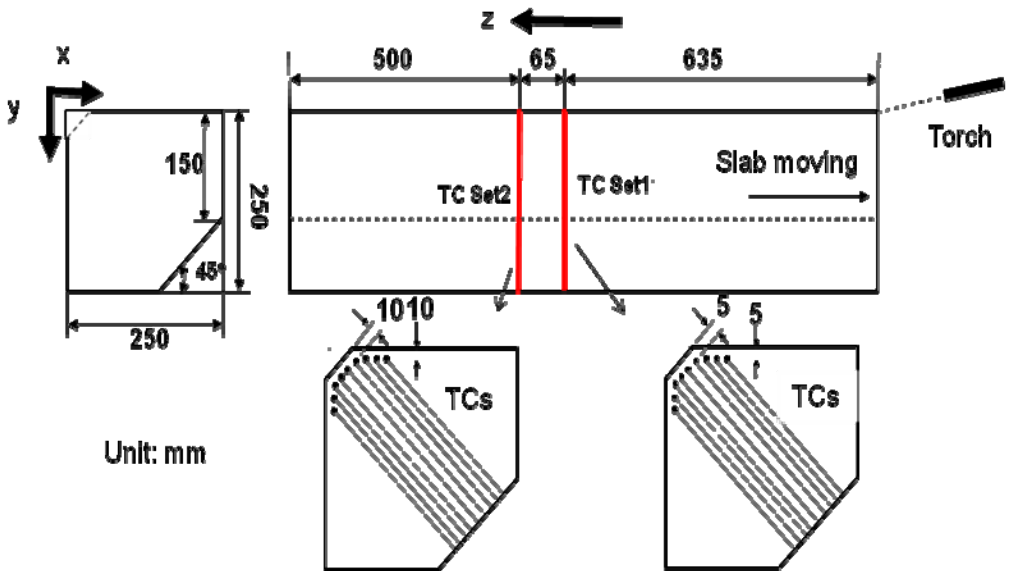

Fig. 4 Initial Slab Dimensions and Thermocouple Locations (t=-50s)

During the experiment, the torch was held stationary pointing at the slab edge at an angle of 5.655^{o} between the torch axis and the slab edge, as shown in Fig. 5. After holding for

~40s of preheating with the torch tip 120 mm from the slab corner, the slab was moved towards the torch at a constant speed of 48.55 mm/s. The TCs temperatures were recorded with time, with the first, shallower TC set 1 naturally heated up earlier and hotter than the deeper TC set 2.

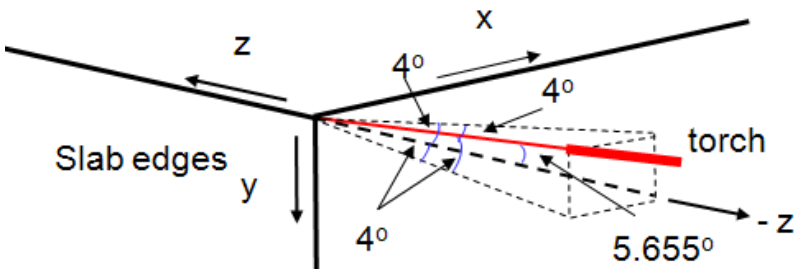

Fig. 5 Torch Orientation relative to Slab Corner

A second experiment was conducted under identical conditions, and the process was stopped suddenly (within 1s). The scarfed surface near the slab edge was sliced carefully along x-y plane. The typical three-dimensional profile of the scarfed surface near the slab edge is shown in Fig. 6. Typical cross sections in the x-y plane are photographed in Fig. 6 (a) and (b). The surface contour compiled from many such cross-sections is given in Fig. 6 (c), including the transition between the scarfed and unscarfed regions of the slab corner, which is about 180mm long. The scarfed surface is obviously not symmetric about the diagonal plane, so asymmetric heat transfer boundary conditions are required to model this experiment.

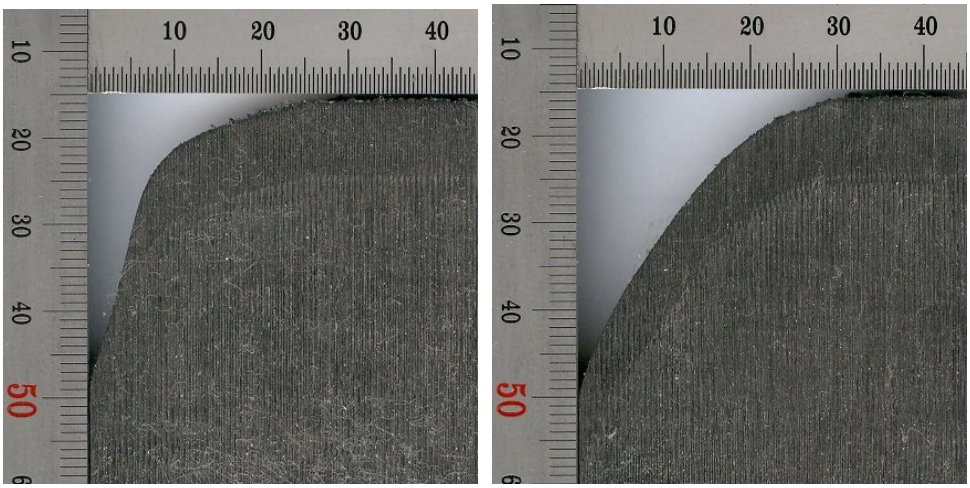

(a) (b)

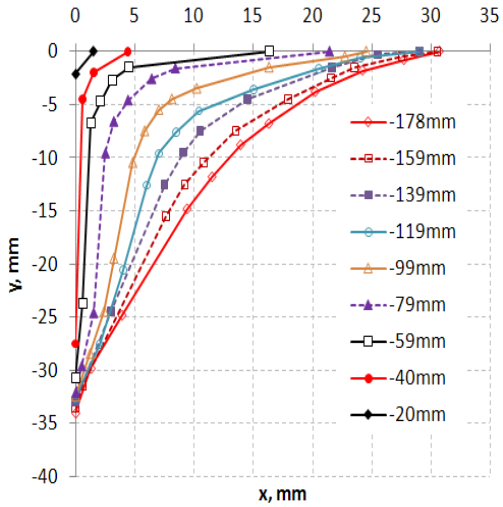

(c)

Fig. 6 a,b) Typical Scarfed Cross-Section Profiles (z= -99mm, -178mm),
b) Final Scarfed Profile (z=-178mm), c) Scarfed Surface Profiles

Section IV. Model Details

A two-step model of heat transfer in the steel slab during the scarfing process has been developed using the commercial software FLUENT [14]. The two domains are shown in Fig.7. The Step-1 model domain, shown in brown in the bottom right, is a small (595mm long) portion of the slab along the scarfing edge.

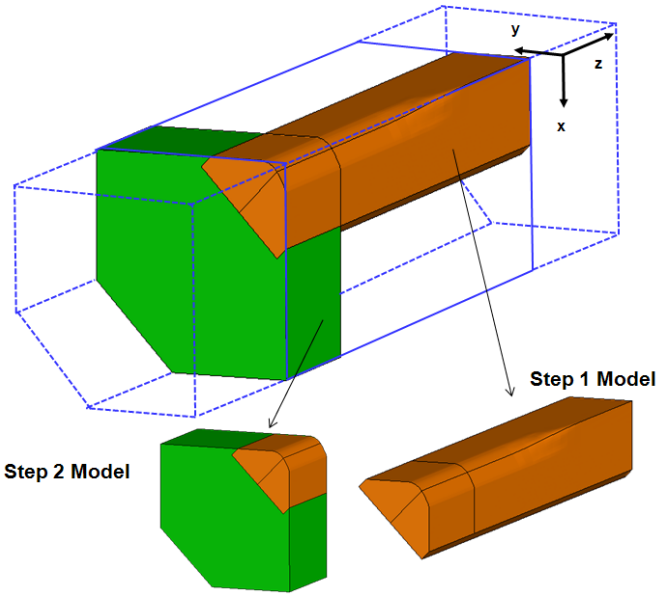

Fig. 7 Two-step Model Domains

The Step-2 model domain, shown in the bottom left, is a 133.2-mm thick slice through the entire slab cross section and includes the left portion of the Step-1 domain. Each step uses a different calculation, as explained next.

IV-1 Step-1 model

The Step-1 model uses a steady-state Eluerian formulation with the material moving through the domain, while the mesh does not change with time. Like the real process, the torch is held stationary while the slab moves through the combustion flame and past the torch at the constant scarfing speed. Thus, the following steady-state heat conduction governing equation is solved by the model:

$$\rho C_p(T)\, \boldsymbol{V}_{scarf} \cdot \nabla T = \nabla \cdot (k(T) \nabla T) \qquad \text{Eqn. 1}$$

in which the scarfing speed $\boldsymbol{V}_{scarf}$ indicates the heat advection and the heat transfer boundary conditions are held constant with time.

This formulation has the important advantage of not needing any change in slab geometry or boundary conditions with time as scarfing proceeds. The measured shape of the new surface generated after the material is removed by scarfing is used to create the Step-1 model domain. The dimensions of this part of the model domain are compared with the corresponding slab photograph in Fig. 8.

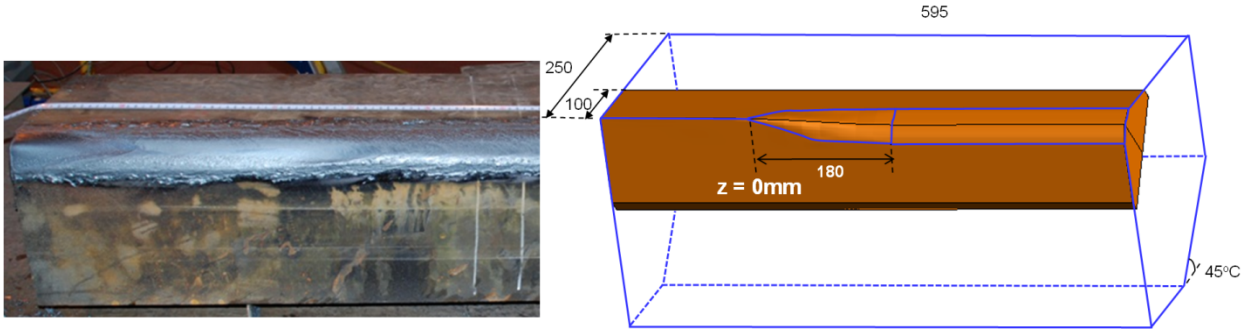

Fig. 8 Left) Scarfed Slab after the Experiment; Right) Step-1 Model Domain and Dimensions

The domain includes only a portion of the slab near the scarfed edge, based on the assumption that heat does not go beyond this domain as the slab moves past the torch. To check validity of this assumption, the analytical solution to a one-dimensional semi-infinite

transient heat conduction problem was checked [15]. Assuming heat flows perpendicular from the slab edge, the solution is valid if the following criterion is satisfied:

$$t<H^2/16\alpha \qquad \text{Eqn. 2}$$

where α is the thermal diffusivity, estimated to be (30 W/mK) / (7400 kg/m3 X 1000 J/kgK) = 4 X 10^{-6} m^2/sec. Taking *t* to be the time for the slab to travel through the domain, (595 mm) / (48.55 mm/sec) =12.3 sec, the domain half-thickness, *H*, is estimated to be greater than 28 mm. This is well-satisfied by the Step-1 model domain, where the top and side surface widths are chosen to be 100 mm and the depth along the diagonal is chosen to be 70 mm.

To define the boundary conditions, the top and side surfaces of the Step-1 model domain are divided into four regions (A, B, C, and D) as shown in Fig. 9. Each region has different heat transfer boundary condition, with the following general form:

$$-k(T)\nabla T=q \qquad \text{Eqn. 3}$$

where ∇T is perpendicular to the slab surface, and q is an applied heat flux (W/m^2). Because the measured scarfing surface is not quite symmetric about the diagonal plane, the boundary conditions are not symmetric either. The positions of the thermocouples in a typical cross section are also labeled in the back face in Fig. 9 where the material exits the domain. In this figure, the shape of the scarfed surface and slab edges is outlined in blue, so extra region labels are added for clarity.

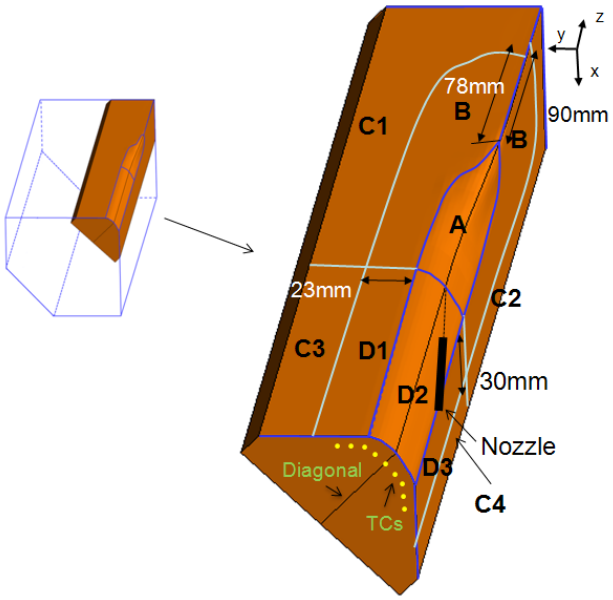

Fig. 9 Step-1 Model Boundary Division

Region A is the scarfing reaction region, where iron reacts with oxygen to form iron oxides and releases heat. The volumetric rate of removal of iron by this oxidation reaction, $\dot{V}_{ox,i}$, is defined for each element area that makes up this surface, A_i, according to the local curved shape of the scarfing surface in this region and the scarfing speed.

$$\dot{V}_{ox,i}(m^3/s) = A_i(m^2)\cos\theta_i V_{scarfing}(m/s) \qquad \text{Eqn. 4}$$

where A_i is the surface element area, θ_i is the angle between the normal to the area and the scarfing axis z, and the scarfing speed, V_{scarf}, is 0.0486m/s.

A portion of the heat generated by this reaction is conducted into the slab, according to the following spatially-dependent heat flux function:

$$q''_{A,i}(\frac{W}{m^2}) = \gamma_{scarfing}\frac{\dot{V}_{ox,i}(m^3/s)\rho_{Fe}(kg/m^3)\Delta H_{scarfing}(J/kg)}{A_i(m^2)} \qquad \text{Eqn. 5}$$

where ρ_{Fe} is the steel density and $\Delta H_{scarfing}$ is the energy released (5.803×10^6 J/kg [Appendix A]) from the reaction between iron and oxygen, as discussed in Section II. In Eqn. 5, $\gamma_{scarfing}$ is a tuning parameter that corresponds to the fraction of this heat that is conducted directly into the steel slab in region A from the scarfing reaction and is found to be 10.3% by matching temperature predictions with the measurements.

Region B is where a layer of hot iron-oxide slag produced by the scarfing reaction coats the slab surface, as shown in Fig. 8 left. In the scarfing process, a new layer of hot slag a' continuously deposits onto the existing (old) slag layer a and propagates forward, as shown in Fig. 10. During a small time interval Δt, in region B, the incremental thickness increase through deposition is Δd.

$$\Delta d = \Delta z \tan(\theta) \qquad \text{Eqn. 6}$$

where

$$\Delta z = \Delta t\, V_{scarf} \qquad \text{Eqn. 7}$$

Δz is the incremental length increase of the deposited layer, and θ is the average angle of inclination of the slag layer in region B. It is estimated by using the scarfing angle near the boundary of region A and B. The rate of increase in thickness can be obtained as:

$$\dot{\zeta}_{slag\_B} = \Delta d/\Delta t = V_{scarf}\ tan(\theta) \qquad \text{Eqn. 8}$$

The average local rate of mass deposition onto an element of surface B is

$$\dot{m}_{slag\_B,i}(kg/s) = \zeta_{dist\_B}\,\dot{\zeta}_{slag\_B}(m/s)A_i(m^2)\rho_{slag}(kg/m^3) \qquad \text{Eqn. 9}$$

where ζ_{dist_B} is a tuning parameter to account for the increase of the slag layer thickness over the length of region B. It increases linearly from 0.2 along the boundary with region C, to 1 along the boundary with region A, because the slag layer gets thinner and more intermittent with distance away from the scarfing region (A). A_i is the element surface area in this region. ρ_{slag} is the slag density. The slag thickness (d) increases from 1mm (at C/B boundary) to 5mm at the A/B boundary. The thickness increase is found by:

d = (V_{scarf} = 0.048m/s) (time spent in region B = 1.63s) tan(θ = 3^o) = 4mm

This result is consistent with the observed angle observed along the top diagonal (where region B is 78-mm long).

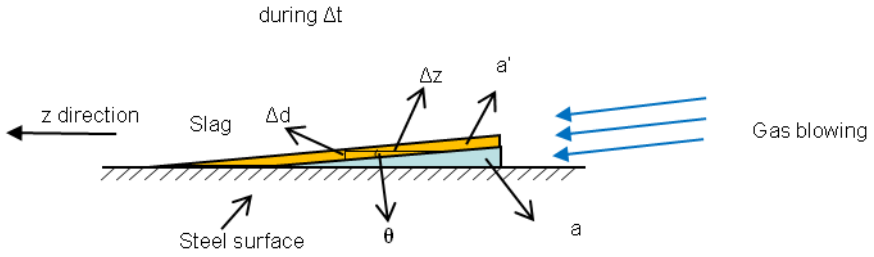

Fig. 10 Schematic of Slag Deposition during a Time Interval Δt

A portion of the heat contained in this hot slag is conducted into the steel slab. Heat flux to the slab surface in this slag coating region B is given in Eqn. 10.

$$q''_{B,i}\left(\frac{W}{m^2}\right) = \gamma_{slag\_B}\frac{Cp_{slag}(J/kgK)(T_A - T_0)(K)\dot{m}_{slag\_B,i}(kg/s)}{(A_i)(m^2)} \qquad \text{Eqn. 10}$$

In Eqn. 10, the area of each surface element in this region, A_i, cancels with the term in $m_{slag,i}$ in the numerator so has no direct effect on the local heat flux. γ_{slag_B} is a tuning parameter that corresponds to the fraction of heat conducted from the hot slag that is deposited onto the slab surface and conducted into the steel slab relative to the total slag produced in region A, and is found to be 5.43% by matching temperature predictions with the measurements; T_A is the

temperature of the slag generated in region A (assumed to be 4000 ^{o}C, as the slag is heated up greatly due to the heat released in the scarfing reaction) and T_0 is the reference temperature which is 0 K.

On the top surface, the width of the slag coating region B increases linearly from 23mm at the boundary with region D to 78 mm at the boundary with the slab edge, as shown in Fig. 9. On the right side surface, it increases linearly from 30 mm to 90 mm. The side coating area is larger than the top area because the side scarfing surface is deeper, which indicates that more material was removed to generate slag. Furthermore, more slag flowed down the side than along the top, due to gravity, and the torch gas momentum.

Region C has no scarfing reaction or slag coating. Regions C1 (top) and C2 (side), are heated by forced convection from the hot, high-speed combustion gases. The detailed model of the combustion and hot gas flow (conducted by Dr. Kim) [16] has revealed that the forced convection heat flux to the slab in region C1 and C2, q_c, varies from 3 X 10^4 W/m^2 to 4 X 10^5 W/m^2 according to position in the non-slag-coated regions of the slab surface, where high speed gas impinges, as shown in Fig. 11, taken from Kim [16]. Parametric studies assuming constant q_c found that the heat transfer results had negligible change when varying q_C between these two extremes. Thus, for simplicity, a average heat flux q_C of 2 X 10^5 W/m^2 was specified in regions C1 and C2.

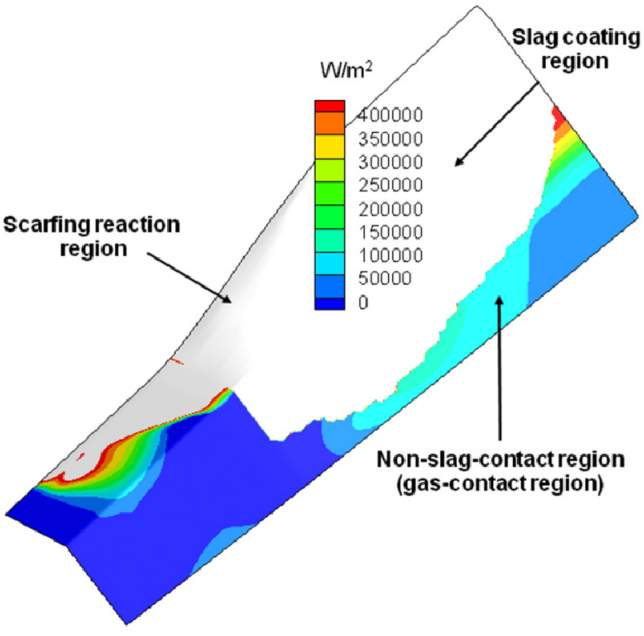

Fig. 11 Heat Flux Distribution along Non-slag-contact Region [16]

Region C3 and C4 are not heated by the hot combustion gas. However, the gas over region C3 and C4 was sucked into region C1 and C2 during the experiment, which increased convection a lot. Therefore, an estimated heat transfer coefficient (100 W/m^2K) greater than natural convection is specified in region C3 and C4.

Region D also has a slag coating. The spatially-dependent heat flux $q_{D,i}$ in region D can be derived analytically and physically from a simple heat balance as shown in Fig. 12.

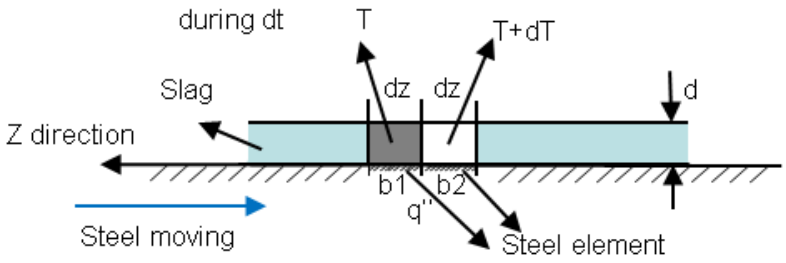

Fig. 12 Schematic of the Slag Contact for Deriving Boundary Heat Flux

The slag thickness is constant (d) in region D. During the time interval dt, the infinitesimal steel element (dz) at b1 moves to b2 and heat increment (dQ) is conducted to this element as calculated by Eqn.11.

$$dQ\ (J) = q''(z)\ (W/m^2)\ dz\ (m)\ dw\ (m)\ dt\ (s) \qquad \text{Eqn. 11}$$

where $q''(z)$ is the spatially-dependent heat flux to the steel slab from the hot slag; and dw is the element width. The heat dQ can also be obtained in Eqn. 12 through the heat decrease in the slag while it contacts the steel element.

$$dQ\ (J) = \gamma_{slag\_D}\ \rho_{slag}\ (kg/m^3)\ Cp_{slag}\ (J/kgK)\ (T-(dT+T))\ (K)\ (\ dz\ dw\ d)\ (m^3) \qquad \text{Eqn. 12}$$

where γ_{slag_D} represents the fraction of heat conducted into the steel slab from the slag. Inserting Eqn. 12 into Eqn. 11, and considering the relationship between distance and time:

$$dz = V_{scarf}\ dt \qquad \text{Eqn. 13}$$

gives the heat flux.

$$q''(z) = \gamma_{slag\_D}\ \rho_{slag}\ Cp_{slag}\ d\ V_{scarf}\ (dT\ /\ dz) \qquad \text{Eqn. 14}$$

Finally, inserting a function to define slag thickness gives the following function for heat flux of each steel element *i* in region D:

$$q''_{D\_i}(z_i)\left(\frac{W}{m^2}\right) = \gamma_{slag\_D}\rho_{slag}(kg/m^3)Cp_{slag}(J/kgK)\zeta_{dist\_D}\zeta_{slag\_D}(m)V_{scarf}\frac{dT}{dz_i} \qquad \text{Eqn. 15}$$

where γ_{slag_D} is calibrated to decrease from 36 % at the entrance of region D to 18% at the exit of region D by matching temperature prediction with thermocouple measurements. (The remaining heat in the slag is lost through convection and radiation.) ζ_{slag_D} is the slag thickness of 5 mm at exit of region B. ζ_{dist_D} defines the thickness decrease along the y direction on the top slab surface and along the x direction on the side slab surface. It has a constant value of 1 in region D2, and decreases linearly from 1 (at D2/D1 and D2/D3 interfaces) to 0.2 (at D1/C3 and D3/C4 interfaces), which almost matches the transverse thickness profile exiting region B, ζ_{dist_B}. dT/dz_i can be approximated to be $(T_{B/D}-T_{D/Step\text{-}2})/\Delta z_D$, where $T_{B/D}$ is the temperature (1900 ^oC) of the slag as it enters region D (D1, D2 and D3), $T_{D/Step\text{-}2}$ is the slag temperature (1100 ^oC) as it exits region D and Δz_D is the length of region D (266.4mm).

The front face where the steel enters the model domain is given a constant temperature of 17 ^oC as the heat transfer boundary condition. The ambient temperature in the room where the experiment was performed was 5 ^oC. The slab temperature before the experiment was around 5 ^oC. However, as the slab moved towards to the hot torch flame, the scarfing surface and slag coating areas were heated up instantly and some heat was conducted through the slab to heat up the slab slightly at far-away locations. Moreover, the hot flame could also heat up the slab at far-away locations. Therefore, by the time the material reaches the domain, its temperature is expected to exceed room temperature. According to the measurements shown later in Fig. 22 and 23, all thermocouples increase slowly to around 17 ^oC and then suddenly go up dramatically.

The back face (with labeled TCs) where material exits the domain, the two narrow side surfaces and the bottom surface all have a zero heat flux (insulated) boundary condition.

IV-2 Step-2 model

The Step-2 model shown in the left bottom of Fig. 7 and Fig. 13 simulates a 133.2-mm-long segment of the slab and uses the Lagrangian method to track its transient temperature history. The governing equation for this 3-D transient heat conduction problem is

$$\rho C_p(T)(\partial T/\partial t) = \nabla\cdot(k(T)\nabla T). \qquad \textit{Eqn. 16}$$

For this model, the slab is held stationary while the torch passes by. Therefore, there is no material motion, and time-dependent heat-transfer boundary conditions are needed. This model is needed because the Step-1 model is not physically long enough to provide a sufficiently-long simulation to cool through the temperature range of interest. The Step-2 model domain starts far enough past the scarfing region that its geometry is fixed, and the necessary complication of changing heat transfer boundary conditions with time is relative easy to handle. This Lagrangian formulation is also easily-suited to subsequent stress analysis.

The Step-2 model calculation lasts ~110s and immediately follows the Step-1 model, which provides the first ~12.2s of the temperature histories. The global time is set to 0 when TC set1 passes by the B/A interface at the diagonal in the Step-1 model domain, where the scarfing region A begins). Thus, the initial condition (global time t=9.14 s) is taken from the steady-state results in the corresponding left (downstream, Fig. 7) portion of the Step-1 model where it intersects with the Step-2 model. The remaining part of the Step-2 domain is given an initial temperature of 17 ^{o}C. The entire initial temperature distribution is shown in Fig. 14.

The heat transfer boundary conditions are also shown in Fig. 13. The front and back surfaces have zero heat flux. The left top surface, right side surface, left side surface and bottom surface have natural convection (h = 10 W/m^{2}K, T_{amb}=5 ^{o}C). The boundary conditions for the top right surface and the right top side surface have the slag coating. The corresponding heat flux is

$$q_{2\_slag,i} = q_{D,i}\ \gamma_{time}(t_i) \qquad \text{Eqn. 17}$$

where t_i is given in Eqn. 17 as a function of global time t.

$$t_i = t + \delta z/V_{scarf}\ -9.14 = t' + \delta z/V_{scarf} \quad (\text{where } t' = t - 9.14) \qquad \text{Eqn. 18}$$

where $\gamma_{time}(t')$ is a tuning parameter to account for the time dependency of the heat flux. It is shown in Fig. 15. It represents the drop of heat flux from the slag coating layer to the steel slab

with time, as the slag coating cools down. It decays exponentially from 1 to 0 in 60 sec. It is chosen to make the temperature predictions match the measurements. A time delay is included in t_i to account for the transition between the steady-state Step-1 model and the transient Step-2 model. Specifically, at the front face, t_i starts at 0 in γ_{time} while at a distance of δz from the front face, t_i starts at $\delta z/V_{scarf}$. The maximum time delay is 133.2mm/V_{scarf}=2.74s.

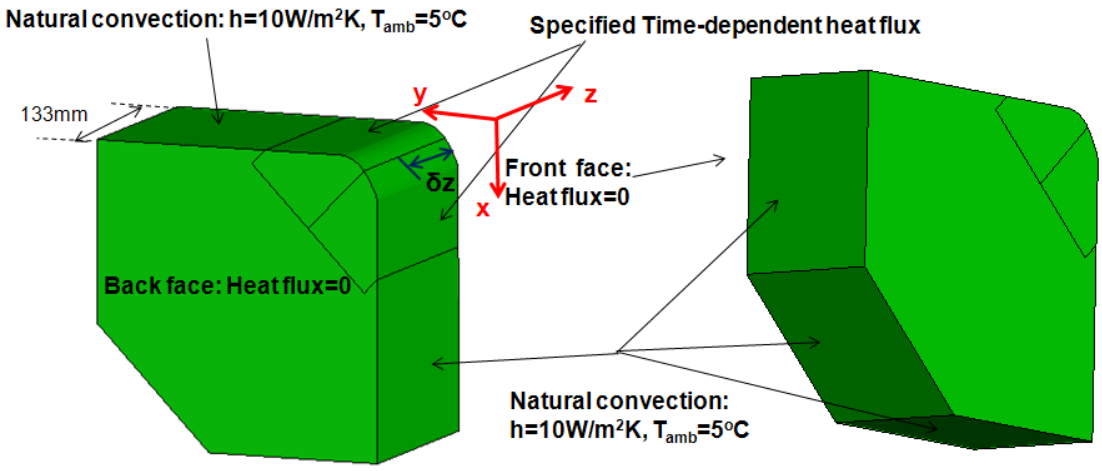

Fig. 13 Step-2 Model Domain, Dimension and Boundary Conditions

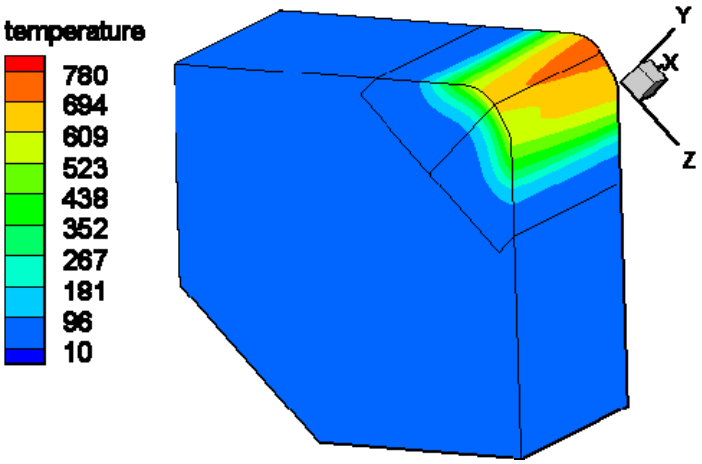

Fig. 14 Initial Temperature Distribution for the Step-2 Model

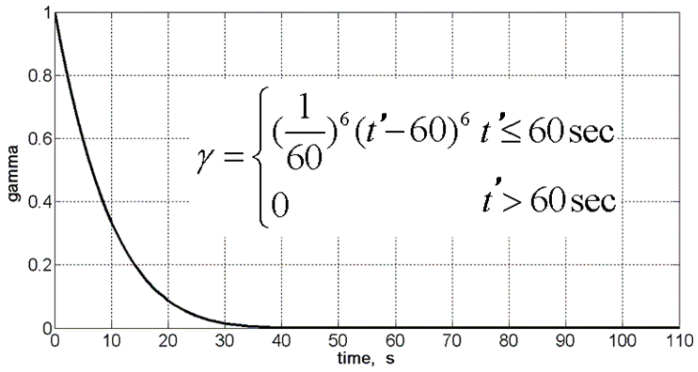

Fig. 15 Time Dependent Heat Flux Tuning Parameter γ_{time}
(note time=0 means global time=9.14s)

IV-3 Numerical Details

The equations were solved using the SIMPLE/ First Order Upwind method in FLUENT. The Step-1 model has 2651616 nodes and 2546600 cells and the Step-2 model has 514941 nodes and 480300 cells. Typical meshes for both models are shown in Fig. 16 (a) and (b) for a slice through the diagonal plane. The meshes are much finer near the scarfing surfaces for both models to capture the sharp temperature gradients there.

10 iterations were needed for Step-1 model, which took 0.5 min of CPU time on a 4.00 G of RAM, 2.67 GHz, Intel(R) Xeon(R) CPU, Dell Precision T3500 computer. Time step size of 0.2s was used for Step-2 model, using the default under-relaxation factor (1). 3 iterations were needed for each time step size in Step-2 model, which took 1.5 sec of CPU time (for 110s transient simulation, total CPU time is around 14 min).

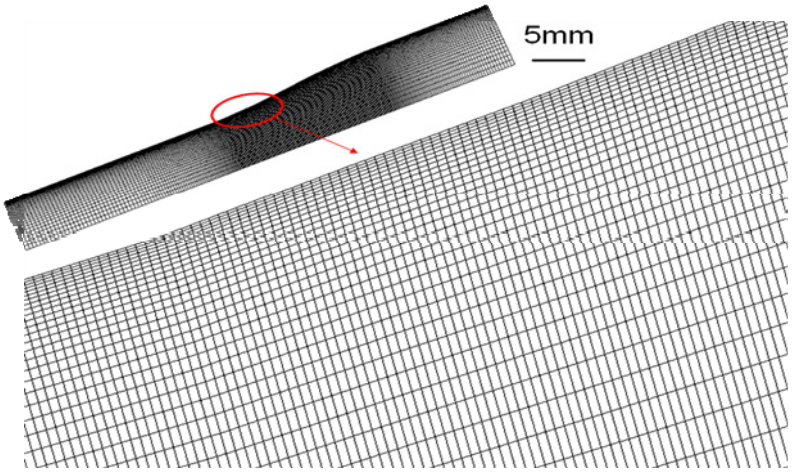

Fig. 16 (a)

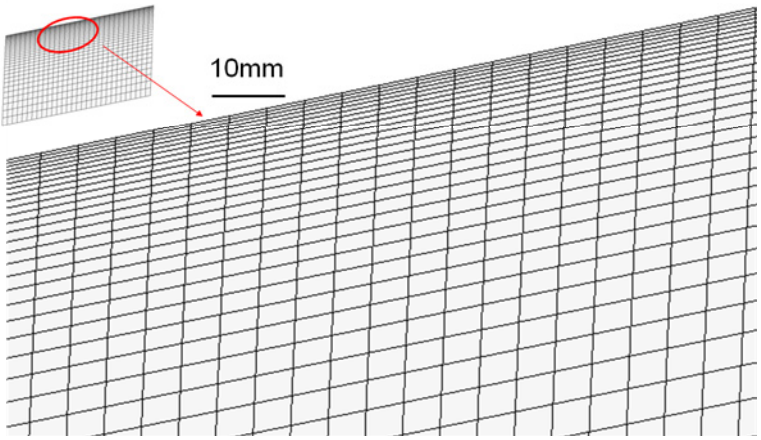

Fig. 16 (b)

Fig. 16 Meshes for the Diagonal Plane near the Scarfing Surface for
a) Step-1 Model and b) Step-2 Model

IV-4 Material Properties

The steel composition in Table 1 was input in the in-house continuous casting simulation code CON1D [17] to calculate the temperature dependent steel thermal conductivity and specific heat, which are shown in Fig. 17 and 18. The dotted lines are input in the model as lookup tables for the heat transfer governing equation calculation. The solidus temperature is calculated to be 1486 ^{o}C and the liquidus temperature is 1516 ^{o}C using the Won segregation model [18] in CON1D.

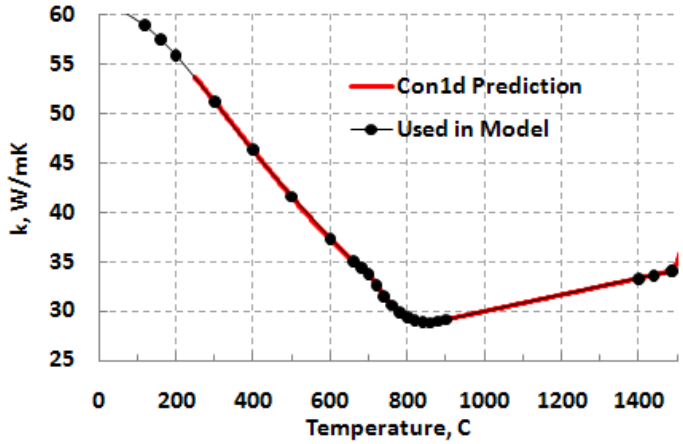

Fig. 17 Steel Thermal Conductivity by CON1D

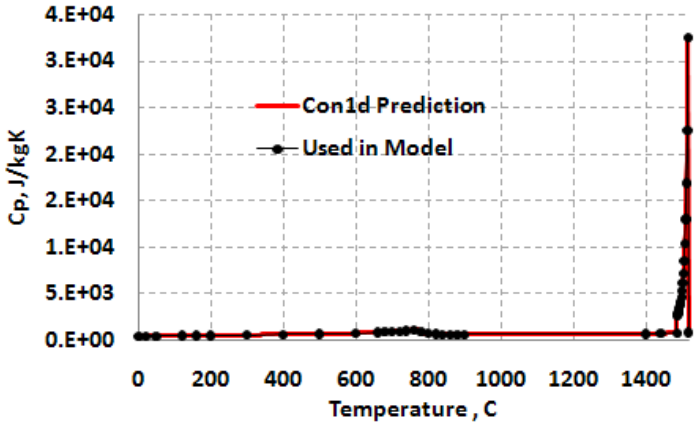

Fig. 18 Steel Specific Heat by CON1D

Slag density is approximately 5100 kg/m^3 [19] and specific heat is 870.4 J/kgK [1]. Gas properties are provided elsewhere, as the results of the combustion and gas flow model were taken from the work of Kim et al [16].

Section V. Results and Discussion

The models were applied to simulate the experiment described in section III. Global time t = 0 is chosen when TC set 1 passes the B/A interface at the diagonal where the scarfing region A begins and is related to events during the experiments and simulations as given in Table 2.

Temperature distributions over the outer surfaces, (slices perpendicular to the z axis and the slices parallel to the z axis) for the Step-1 model are shown in Figs. 19 and 20. In the Step-1 model, most heat is transported from upstream to downstream by simple advection of the moving slab. At the same time, heat slightly diffuses towards both sides, as shown in Fig. 19 (b) and Fig. 20. Temperature is naturally highest at the scarfing reaction region. The maximum temperature (1489 ^{o}C) in the domain is roughly equal to the solidus temperature (1486 ^{o}C), as expected. The high-temperature region of 1100 ^{o}C ~ 1489 ^{o}C is confined to a thin, 0.5mm deep layer in the curved portion of the scarfing reaction region where the torch impinges, as shown in Fig. 20. Heat cannot conduct deeper because the material in this region is quickly removed by the scarfing reaction. Heat is transported to the sides from the combined action of lateral

conduction and heat input from the slag layer. Temperature at the bottom surface and two narrower side surfaces of the Step-1 domain is found to be less than 18 ^{o}C, which validates the assumption taken to create the size of the Step-1 model domain (within 1 ^{o}C of the initial temperature).

Time, s	Events
-50.00	Start of preheating
-9.37	End of preheating
-7.74	Torch end passes the slab corner
-3.06	Thermocouple TC set 1 enters Step-1 model domain (front face)
-1.72	TC set 2 enters Step-1 model domain
0.00	TC set 1 passes B/A interface (at the diagonal line – see Fig. 9)
1.34	TC set 2 passes B/A interface (at the diagonal line)
3.71	TC set 1 passes region A/D interface
5.36, 6.66	Torch end passes TC sets 1, 2
9.14	Step-2 model starts (TC set1 passes back face of Step-2 model domain and stays at back face of Step-2 model domain.)
119.14	Simulation ends

Table 2. Time Line of Events

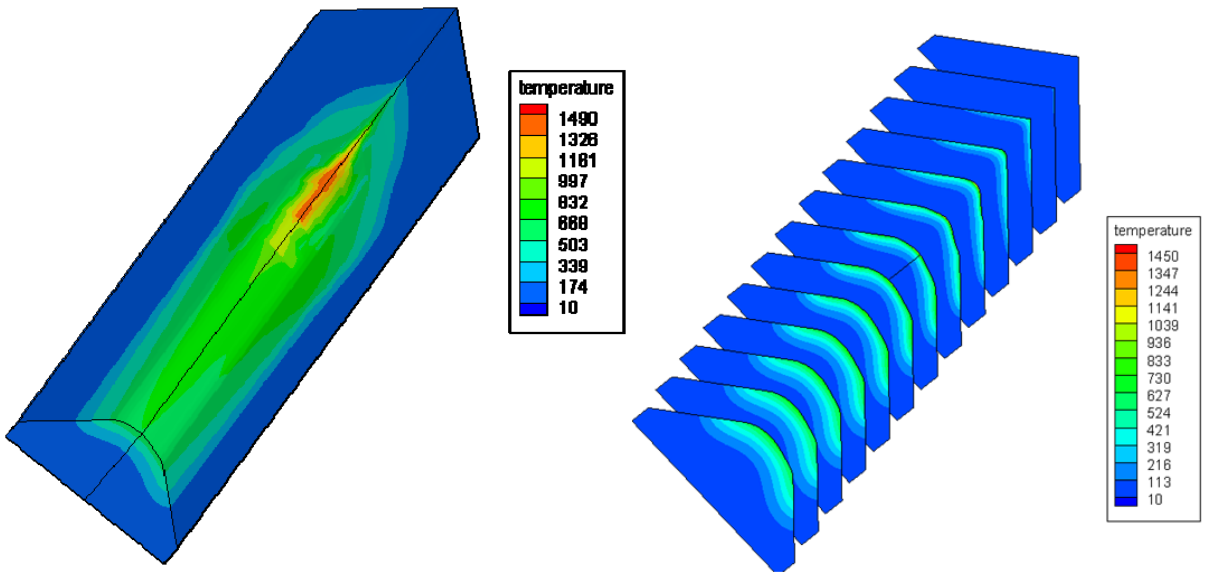

(a) (b)

Fig. 19 Step-1 Model Temperature Distribution along

(a) Outer Surface, (b) Slices Perpendicular to the z Axis

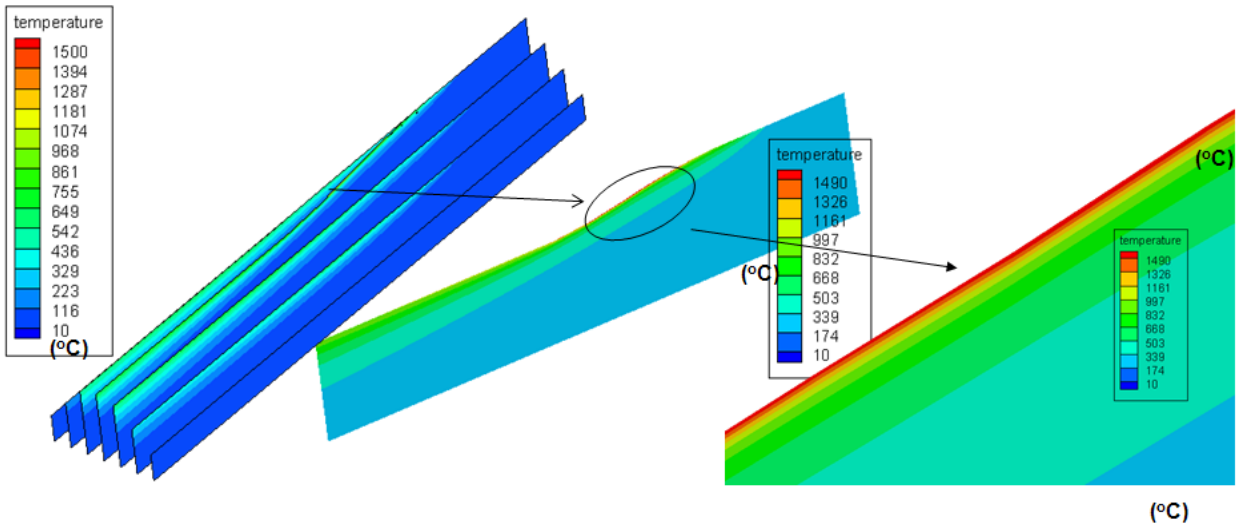

Fig. 20 Step-1 Model Temperature Distribution along Slices

Parallel to the z Axis and Its Zoom-in Contours

The temperature distribution at 119.14 sec for the Step-2 model is shown in Fig. 21. Obviously, the heat affected zone extends beyond the small intersection part that was formerly

part of the Step-1 domain to the remaining slab. This demonstrates the importance of modeling the entire slab cross section with the Step-2 model.

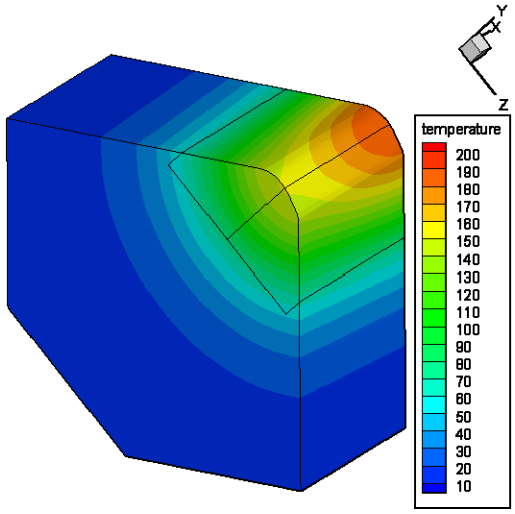

Fig. 21 Step-2 Model Temperature Distribution at Global Time 119.14 sec

The temperature history predictions for the two set of thermocouples are compared with the experimental measurements in Fig. 22 and 23. The corresponding positions of thermocouples in the slab cross section are also labeled. The Step-1 model temperature prediction is separated from the Step-2 model temperature prediction by a vertical solid line. The smooth transition between these two models is further evidence that the model formulation is reasonable.

Predictions match the measurements quite well for both thermocouple depths (set 1 and set 2). The agreement is best for the thermocouples close to the scarfing symmetry plane while the match is still good for the thermocouples further away from the edge across the top and side. As shown clearly in Fig. 3, as the slag layer extends further away from the scarfing surface, it scatters randomly and some locations are covered with a thick layer while other locations are not coated with the slag. The two-step model only models the average effect of the slag coating layer. Therefore, it is reasonable and expected that thermocouples farther away from the scarfing surface and likely experience more variability and so are much more difficult to match well.

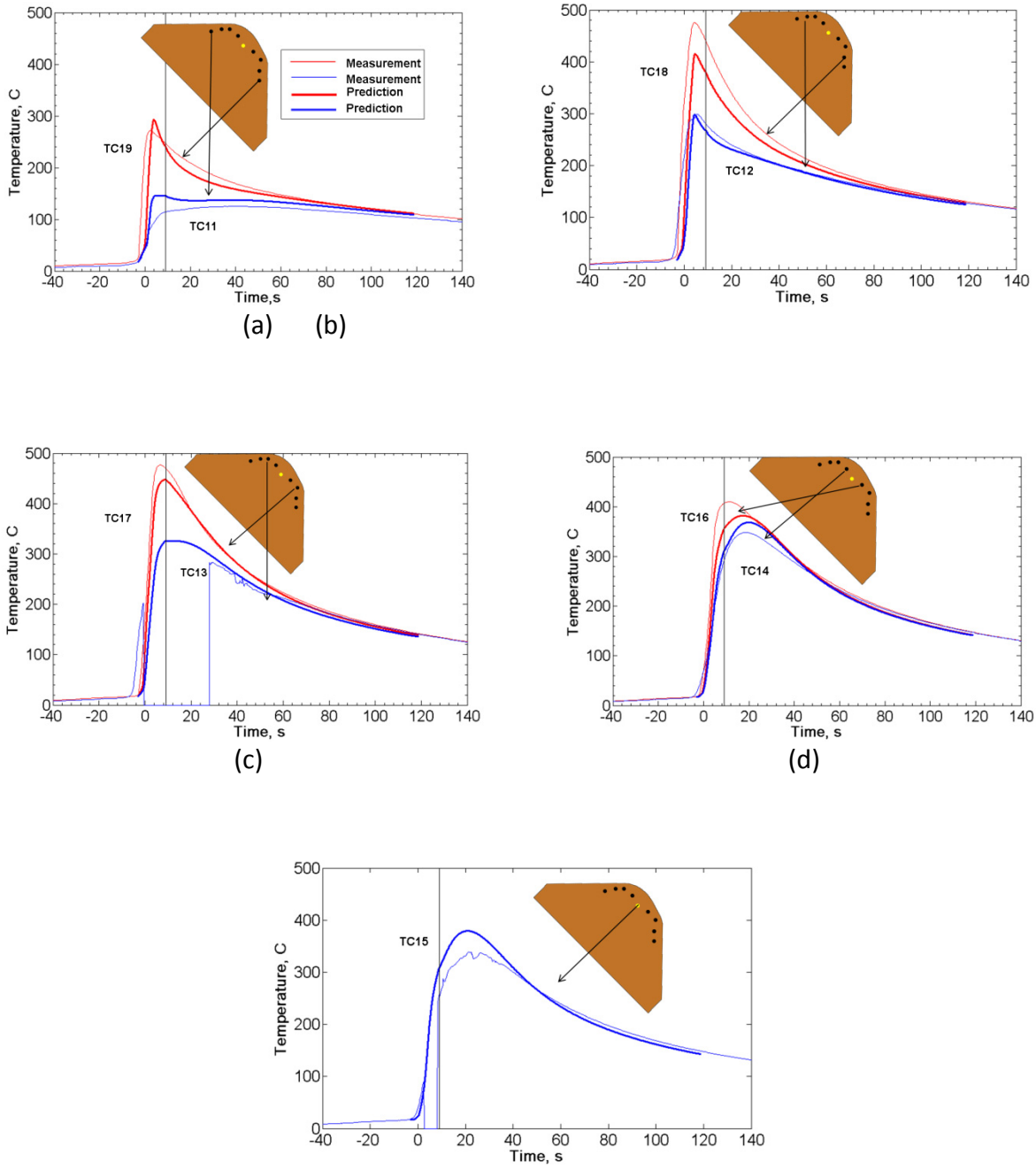

Fig. 22 Comparison between Predictions and Measurements for TC Set 1

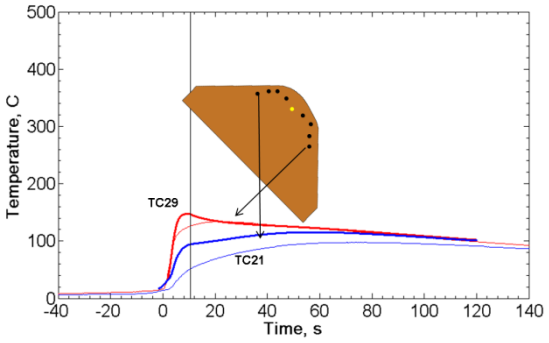

(a)

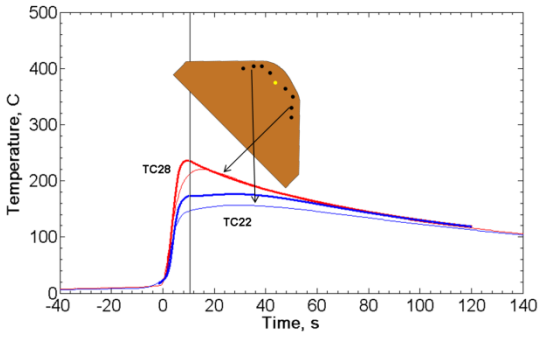

(b)

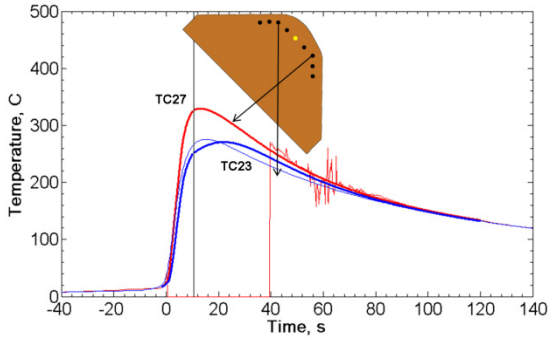

(c)

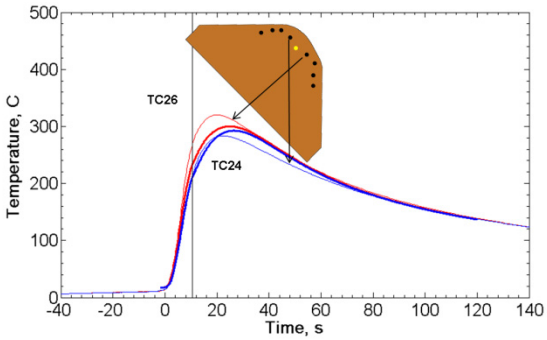

(d)

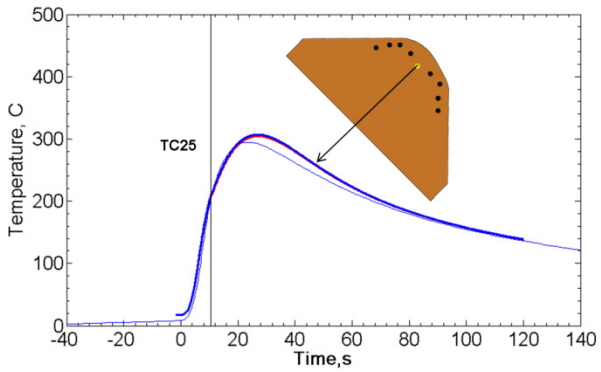

(e)

Fig. 23 Comparison between Predictions and Measurements

for TC Set 2 (vertical solid line separates results from Step-1 and 2 models)

The boundary heat flux distribution is shown in Fig. 24 (a), (b) and (c). It is obvious that heat flux is dependent on the region where different heat flux specification has been applied. Region A gives the largest heat flux, with over 30 MW/m^2 peak. Region B gives the second largest heat flux, followed by regions D1, D2, D3, C1, C2, C3 and C4 (which has the smallest heat flux of ~1 MW/m2). The heat flux distributions along seven transverse paths and seven longitudinal paths are shown in Fig. 26 and 27, respectively. These longitudinal and transverse paths are clearly labeled in Fig. 25. The heat flux discontinuity with region A or B is caused by the discontinuity within curved surface (scarfed surface) or the discontinuity of the heat flux tuning parameter ζ_{dist_B}. The heat flux discontinuity between region A and region D is caused by the discontinuity of the measured surface slope, which is shown in Fig. 28. The sudden transition to a flat surface suddenly eliminates the scarfing reaction heat source.

The temperature distributions along the seven transverse and seven longitudinal paths are shown in Fig. 29 and Fig. 30, respectively. Note that these paths follow the slab surface, so are not straight lines. Temperature profiles are more continuous than the heat flux profile, especially with increasing depth below the slab surface, due to thermal diffusion. As seen in Fig. 29, the temperature profiles are not symmetric about the diagonal, which is due to the asymmetric shape that controls the heat generated by the scarfing reaction. In Fig. 30, the temperature of the slab surface goes up gradually from 17 ^{o}C to around 80 ^{o}C by heating of the combustion gas, and then it goes up quickly in region B, where slag heating plays an important role. After region B, steel enters region A for path 0, 1 and 2 or into region D for the off-diagonal path 3. The temperature wiggles along paths in region A are caused by the discontinuity of the surface heat flux caused by the slight wiggles in the discretization of the surface shape measurements. In the end, all temperatures decrease slowly in region D.

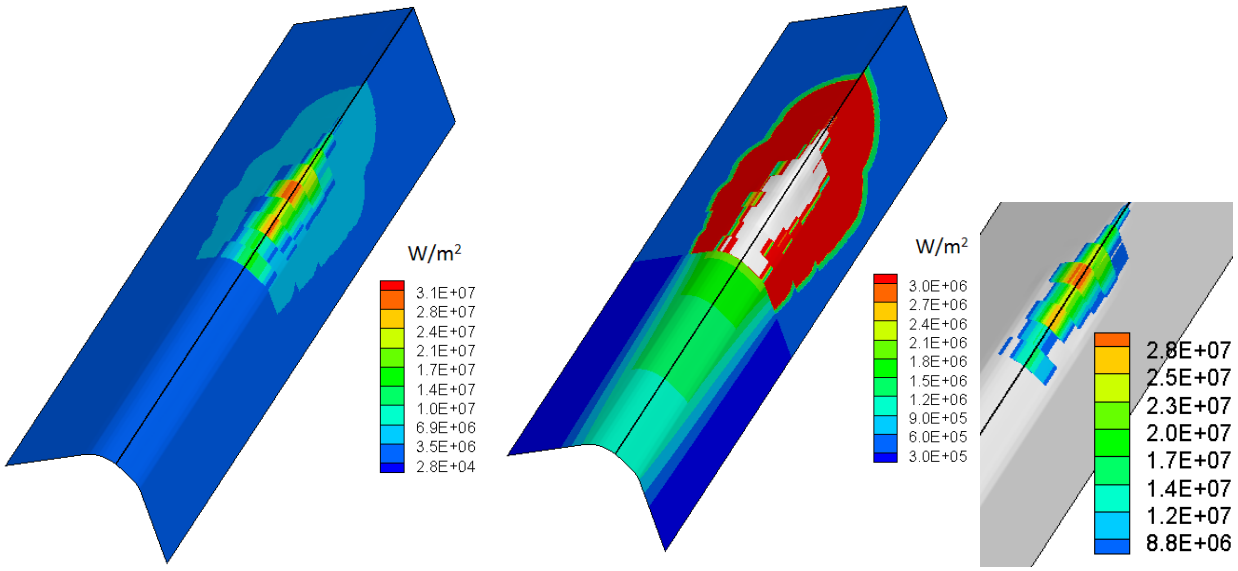

(a) (b) (c)

Fig. 24 Heat Flux Distribution over the Slab Surface

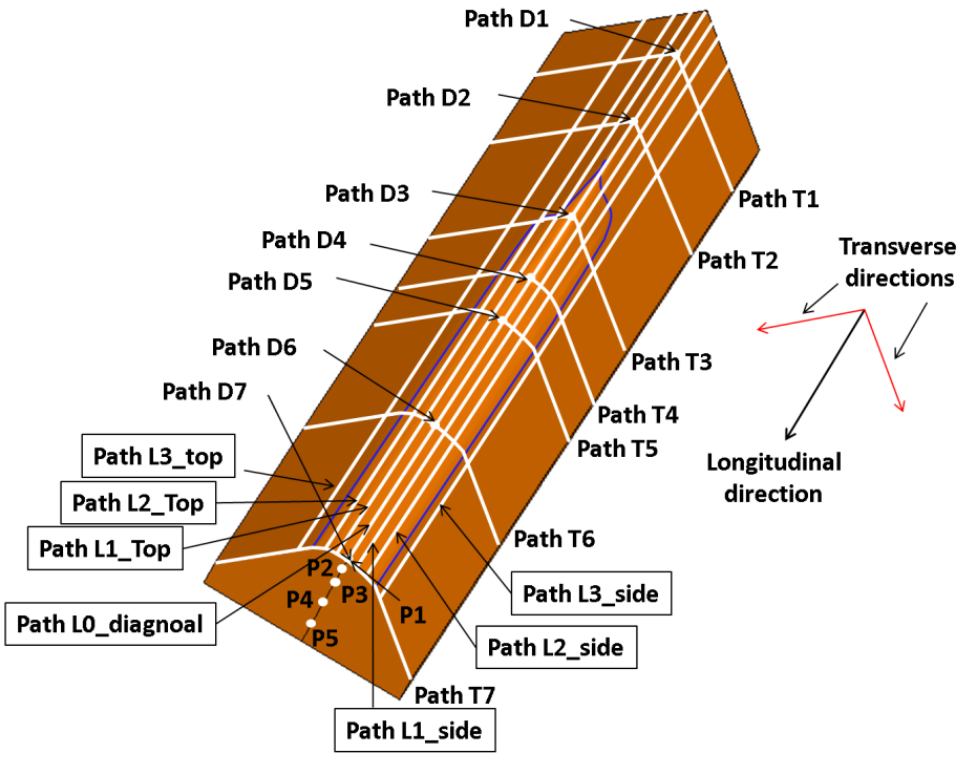

Fig. 25 Schematic of Seven Longitudinal, Transverse and Diagonal Paths and 10 Locations

(note axis label origin indicates time=0)

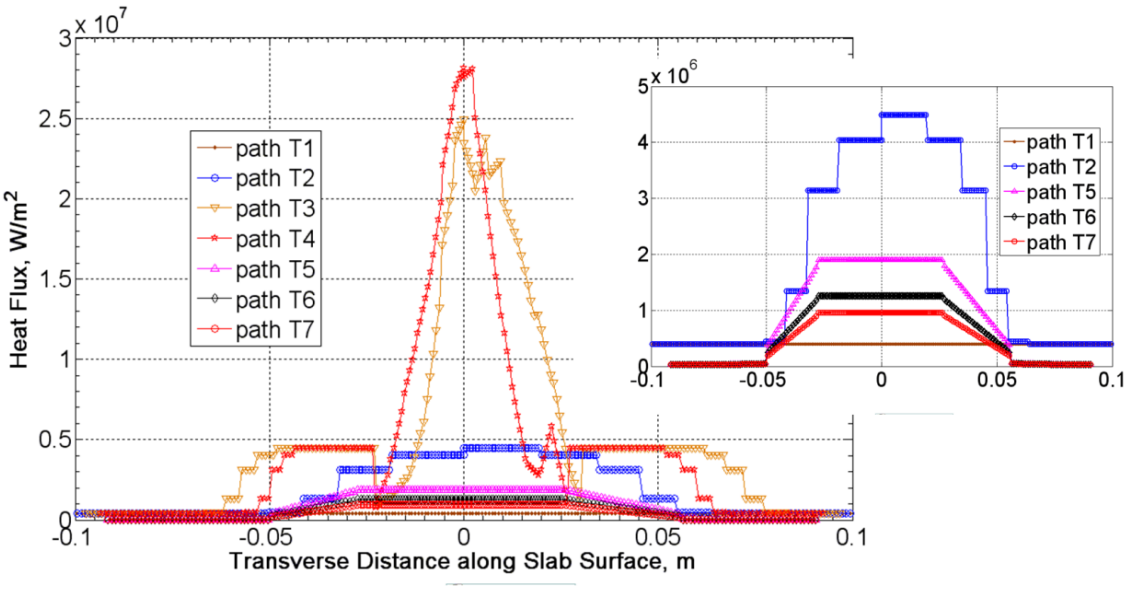

Fig. 26 Heat Flux Distributions (and Zoom-in) along

Seven Transverse Paths around Slab Surface (0=diagonal)

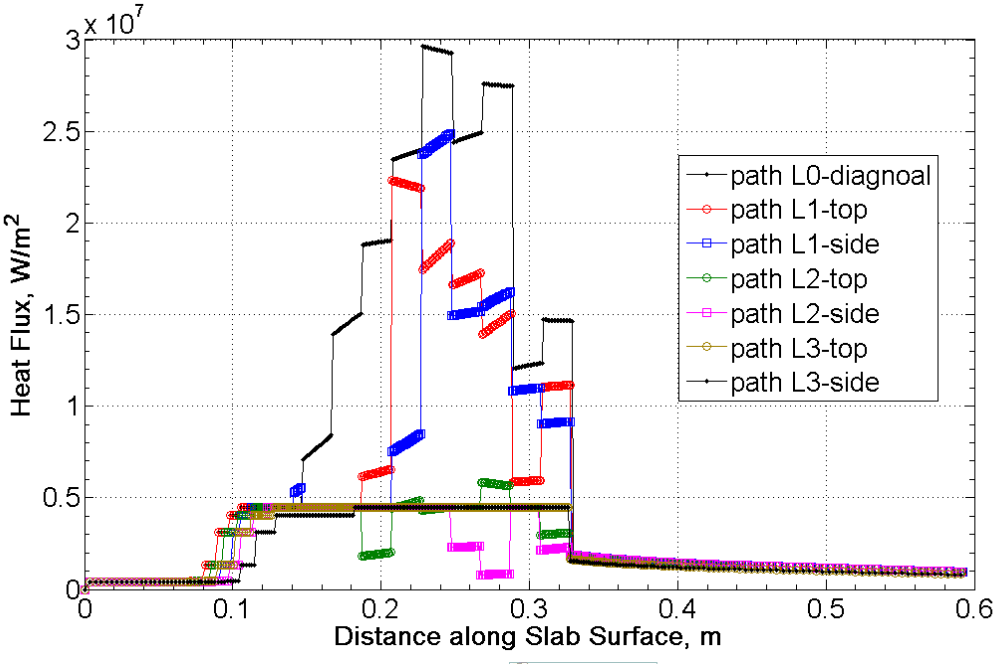

Fig. 27 Heat Flux Distribution along Seven Longitudinal Paths along Slab Surface

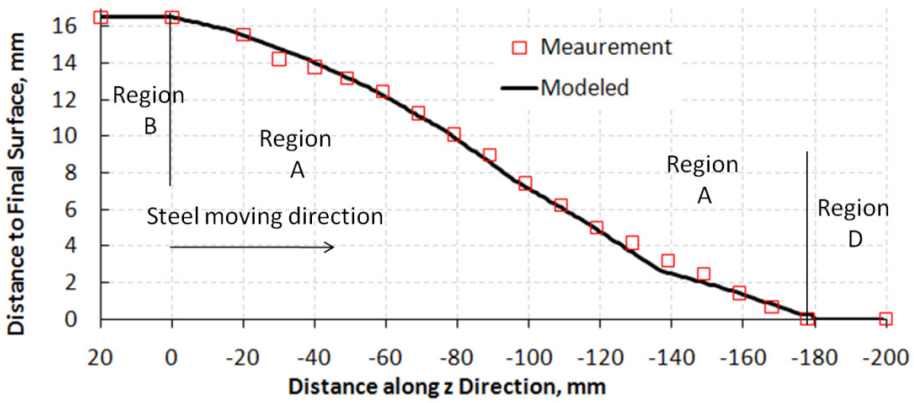

Fig. 28 Surface Profile (Distance to the Scarfed Surface) along Path L0-diagnoal (Fig. 20.2) from Measurement and Modeling (note distance z = 0 corresponds to time=0)

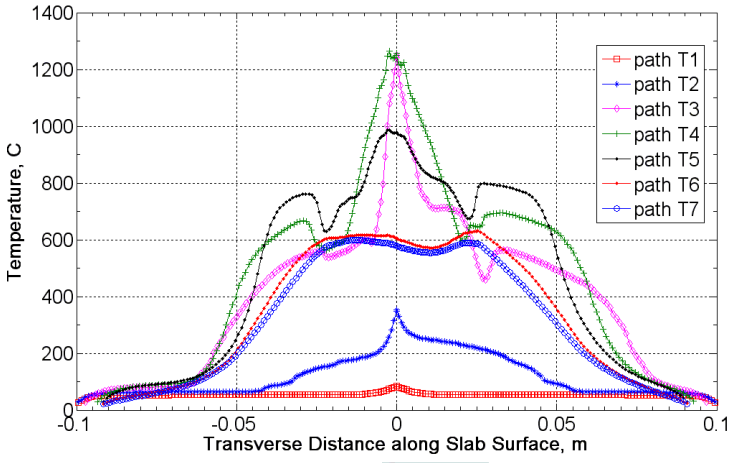

Fig. 29 Temperature Distribution along Seven Transverse Paths around Slag Surface

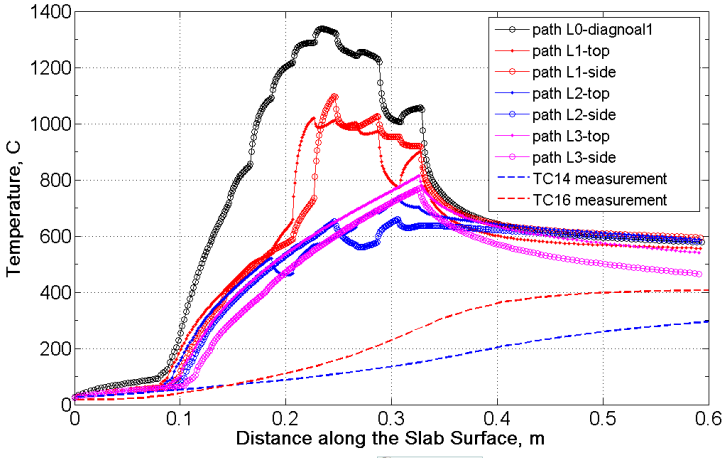

Fig. 30 Temperature Distributions along Seven Longitudinal (z) Paths along Slab Surface

In Fig. 31, seven temperature profiles are shown along the paths which lie in the diagonal plane, perpendicular to the scarfing surface, and are indicated by the locations 1 to 7 in Fig. 25. The distance along the diagonal from the surface (depth below the surface) is chosen to be 0 at the final scarfed surface. Positive distances indicate location in the un-scarfed material (or remaining material) and negative distances indicate the depth into the final slab. As the steel moves towards the torch, its temperature increases gradually from path 1 to path 2 due to the heating of combustion gas in regions C1 and C2. From path 2 to path 5, the temperature near the surface increases quickly due to the scarfing reaction in region A. As the steel moves out of region A, its high temperature part is removed by the scarfing reaction. As it moves through region D, the surface temperature decreases from 1000 ^{o}C to 600 ^{o}C, but the inner slab temperature increases gradually due to heat conduction penetrating from the hot region near the slab surface. Another finding is that the steel deeper than 50mm is not much affected, which again confirms the Step-1 model domain size assumption, as mentioned in Section IV (a).

In Fig. 32, temperature histories are given for positions P1, P2, P3, P4 and P5 (corresponding to depths of 0 mm, 2 mm, 10 mm, 30 mm and 50 mm, respectively, beneath the scarfing surface along the diagonal, relative to the final scarfed surface=0). The calculations and measurements together present a consistent illustration of the temperature history variation with depth beneath the slab surface. The wiggle observed at the beginning of Step 2 model prediction in 0 mm and 2 mm curves is caused by the inconsistency of surface heat flux functions between region D and the Step-2 model. Note that the surface temperature (P1) increases sharply after reaching the torch (time 0). With increasing depth, there is an increasing delay before the TC “feels” the heat diffused from the scarfed region. Also note that the heatup of TC25 (measurement) is further delayed by 1.34s, owing to its different z-position along the length of the slab, which was not compensated for the simulations for this figure, which are all for TC set 1. (This causes a slight offset between the prediction and measurement at 17.5mm, relative to the comparison in Fig. 23e).

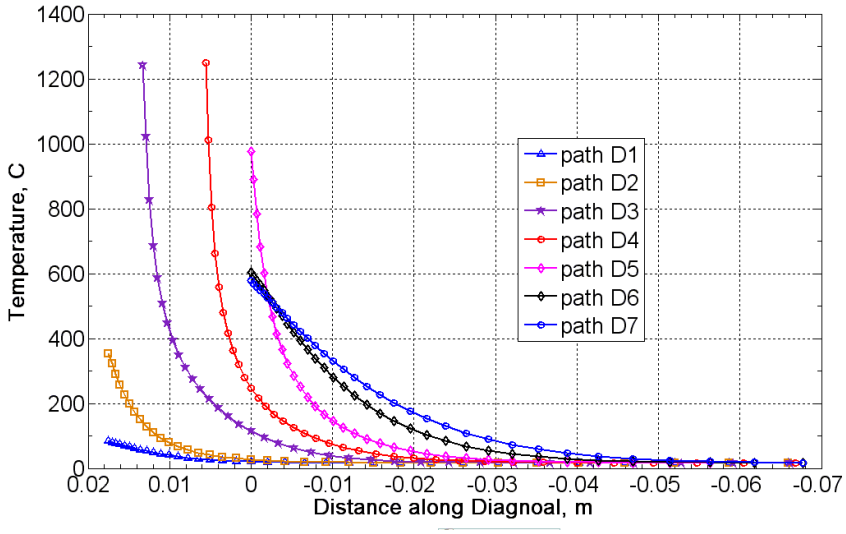

Fig. 31 Temperature Distributions along Seven Transverse Diagonal Paths

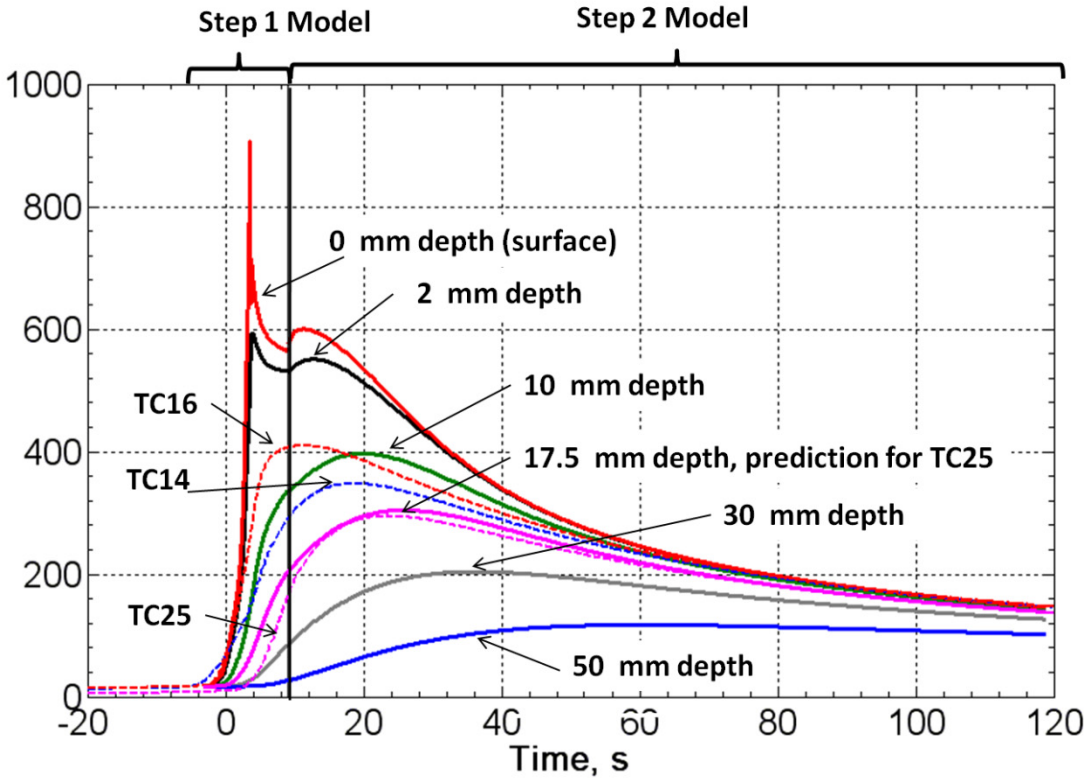

Fig. 32 Temperature Histories for Positions P1-5 (at z-distance of TC set 1) and Measurements from TC14, TC16 and TC25 (simulated lines are solid; measured lines are dotted)

It is interesting to note from these temperature histories of the final slab in Fig. 32 that the maximum temperature along the diagonal is ~900 ^{o}C, and the region of the final slab surface that transforms to austenite (and thus has a danger of martensite formation upon cooling) is less than 2mm. If martensite formation occurs, the expansion of the surface martensite might cause subsurface tensile stresses that could generate subsurface cracks in a worst-case scenario. However, the maximum cooling rate is found on the surface, on the order of 10 ^{o}C/s, so this scenario is unlikely unless the steel is highly alloyed.

Section VI. Summary

A novel two-step model is developed in Fluent and applied to simulate three-dimensional heat transfer during the scarfing processing. This efficient and accurate model includes detailed heat-transfer boundary models for the scarfing surface and the slag coating surfaces. The two-step model combines an Eulerian model of steady heat transfer in the initial scarfing region (12.2s) with a Lagrangian model of transient heat transfer during subsequent cooling of the slab, (110s) to get comprehensive temperature predictions of the entire process for 122.2 sec. The temperature predictions match reasonably well with the thermocouple measurements. The fraction of heat from the scarfing reaction to the slab is found to be 10.3% while that from the slag coating layer is 5.4%. A high temperature region of 1100 ^{o}C to 1489 ^{o}C is found very near to the scarfing surface, and extends to a depth of only 0.5 mm. A very fine mesh resolution (element thickness <0.5mm) near the surface is required in the numerical calculations in order to capture the high temperature gradients in this thin region, and there may still be accuracy issues there. It is found that the heat from the scarfing reaction and the consequent slag coating dominates the temperature evolution while the forced convection by the high speed and high temperature flame and combustion gases does not affect heat transfer very much. Surface temperature of the final slab reaches a maximum of ~900 ^{o}C, with a maximum cooling rate of ~10 ^{o}C/s. The results clearly explain the temperature histories recorded by the thermocouples and have implications for stress and crack formation.

Section VII. Future work

Stress analysis based the current heat transfer results should be performed using ABAQUS to check if there is any residual stress accrued during scarfing to form new cracks. Combustion simulation combined with heat transfer modeling should also be performed to reveal more practical insights, such as how the scarfing speed relates to the steel removing rate or scarfing depth.

Section VIII. Acknowledgement

The authors would like to thank the Continuous Casting Consortium for the support of this project, especially the funding from POSCO. The authors would like to thank Dr. Seong-yeon Kim for this previous intensive research investigation on the scarfing processing simulation. The authors would also like to thank POSCO researchers for carrying out the scarfing experiment, and ANSYS Inc. for supplying FLUENT.

References

[1] “The Making, Shaping and Treating of Steel”, 10th Edition/Latest Technology, Published by Association of Iron and Steel Engineers, pp. 369-377, 1984

[2] T. A. Steinberg, G. P. Mulholland, D. B. Wilson and F. J. Benz, “The combustion of Iron in High-Pressure Oxygen”, Combustion and Flame, vol. 89, pp. 221-228, 1992

[3] T. A. Steinberg, H. D. Beeson and B. E. Newton, “Discussion on Steel Burning in Oxygen (from a Steelmaking Metallurgist’s Perspective)”, Flammability and Sensitivity of Materials in Oxygen-Enriched Atmosphere, Vol. 9, ASTM STM 1395, American Society for Testing and Materials, West Conshohocken, PA, 2000.

[4] A. Pfeuffer, “Development of Scarfing Equipment”, Iron and Steel International, v48, n2, p 145, 147-151, Apr 1975

[5] O. Hintz, R. Blackbourn, “Recent Development in Machine Scarfing of Continuous Cast and Rolled Steel”, Iron and Steel Engineer, v55, n1, p 68-71, Jan 1978

[6] A. Veis, V. Palko, Y, Zimin, P. Soloveichik, L. Safronovich and G. Savelev, “Mechanized Line for Flame Scarfing of Cold Slabs”, Steel in the USSR, v11, n12, p 659-661, Dec 1981

[7] J. Lin, H. Wang and C. Liu, “Energy Saving in Machine Scarfing Operation”, South East Asia Iron & Steel Inst, 1984

[8] O. Synnergren, “Spot Scarfing of Steel Slabs”, Metallurgiska Forskningsstationman, p 10.1-10.11, 1984

[9] G. Klaybor, R. Smith and M. Showalter, “Machine Scarfing and Steel Conditioning in 1990’s”, Iron and Steel Engineer, v70, n9, p 31, Sep 1993

[10] E. Evertz, “Impulse Torch for Energy-saving Slab Scarfing”, MPT Metallurgical Plant and Technology International, v30, n4, p 50-53, Sep 2007

[11]J. Rawson, C. Foster, S. Jose and R. Ratcliffe, “Metallurgical Study of In-Line Hot Scarfing”, Commission of the European Communities, British Steel Corp, 9, Albert Embankment, GB-LONDON SE17SN, Contact No. 7210-EA/809, 1987

[12] M. Showalter, V. Nemchinsky and J. Khan, “Fundamental Study of Oxygen Scarfing Process”, HTD-Vol. 332, National Heat Transfer Conference, Volume 1, ASME, 1996

[13] http://www.posco.co.kr

[14] http://www.fluent.com/

[15] J. Danzig and C. Tucker's book "Modeling in Materials Processing", Cambridge University Press, P94-97

[16] S. Kim and B. G. Thomas, "Design of In-line Edge Scarfing Nozzle Using Numerical Analysis", Final Report, POSCO-UIUC Joint Research, Jan 2008

[17] Meng, Y. and B.G. Thomas, "Heat Transfer and Solidification Model of Continuous Slab Casting: CON1D",Metallurgical & Materials Transactions, Vol. 34B, No. 5, Oct., 2003, pp. 685-705.

[18] Y. Won and B. G. Thomas, "Simple Model of Microsegregation During Solidification of Steels", Metallurgical and Materials Transactions A, Vol. 32A, No. 7, pp. 1755-1767, Jul 2001

[19] http://www.micmet.com/iron_oxide_black.htm

Appendix

A. Calculation of released heat during the exothermic scarfing reaction ($3Fe+2O_2=Fe_3O_4+\Delta_rH^{\Theta}_T$)

	Standard reaction enthalpy change	Cp=a+bT-cT^{-2} (Cal/mol C)				
	$\Delta_rH^{\Theta}_{298}$ (Cal/mol)	a	b *10^3	c *10^{-5}	Temperature range, deg C	Phase transformation energy(Cal/mol)
Fe	0	3.04	7.58	-0.6	25-769	326 @ 769 deg C
		11.13	0	0	769-911	215 @ 911 deg C
		5.8	1.98	0	911-1392	165 @ 1392 deg C
		6.74	1.6	0	1392-1537	3670 @ 1537 deg C
		9.77	0.4	0	1537-2700	
Fe_3O_4	-267800	21.88	48.2	0	25-627	0 @ 627 deg C
		48	0	0	627-1597	33000 @ 1597 deg C
O_2	0	7.16	1	0.4	25-2700	

The equation for calculating the heat released during a isothermal reaction is given by Kirchhoff, as shown below.

$$\Delta_r H_T^{\Theta} = \Delta_r H_{298}^{\Theta} + \int_{298}^{T_{tr}} \Delta c_p dT + \Delta_{tr} H + \int_{T_{tr}}^{T_m} \Delta c_p^{'} dT + \Delta_{fus} H + \int_{T_m}^{T_b} \Delta c_p^{''} dT + \Delta_b H + \int_{T_{tr}}^{T} \Delta c_p^{'''} dT$$

T_{tr} is the phase transformation temperature; T_m is the melting temperature; T_b is the boiling temperature. Δc_p ($\Delta c_p''$, $\Delta c_p'''$) is the heat capacity difference between reaction products and reactants. $\Delta_{tr}H$, $\Delta_{fus}H$, Δ_bH are the heat associated with the solid phase transformation, fusion and vaporizing, respectively.

For the reaction $3Fe+2O_2=Fe_3O_4$ at 1500 ^{o}C, the released heat is calculated using the above equation to be 232.4 Kcal/mol (972.4 kJ/mol). In terms of the mass of Fe (the released heat kJ per kg of Fe), it is 232.4 Kcal/mol x 4.184 J/cal / 3 / 0.05585 kg/mol = 5803 kJ/kg.